J. Fluid Mech. (2003), *vol.* 489, *pp.* 1–27. © 2003 Cambridge University Press
DOI: 10.1017/S0022112003004440 Printed in the United Kingdom

Computational analysis of the two-dimensional–three-dimensional transition in forward-facing step flow

By DIRK WILHELM, CARLOS HÄRTEL† AND LEONHARD KLEISER

Institute of Fluid Dynamics, ETH Zentrum, CH-8092 Zürich, Switzerland

(Received 27 November 2001 and in revised form 2 January 2003)

Results are presented from a computational study of the flow over a forward-facing step in a plane channel. The aim of the study is to gain better insight into the three-dimensionality that is typically observed in the separation region of flows over steps and ribs, and in similar configurations. We consider laminar flow at a Reynolds number of 330, based on step height and bulk velocity of the oncoming flow, and the step is assumed to be infinitely extended in the spanwise direction. High-resolution simulations are undertaken using a mixed spectral/spectral-element code. Moreover, a linear stability study of the flow at the step is performed. The results show that, in the case considered, the three-dimensionality is not related to some absolute instability of the separation bubble in front of the step; rather, it is a sensitive reaction of the flow to three-dimensional perturbations present in the oncoming stream. It is demonstrated that disturbance amplitudes of less than 1% of the mean flow (at, say, 10 step heights ahead of the step) already suffice to produce a visibly three-dimensional structure of the separation zone. If the disturbance level is systematically decreased, the three-dimensional state evolves to an almost two-dimensional recirculation. Here, the key finding is that the intensity of the flow response is proportionate to the amplitude of the inflow disturbance, meaning that the breakup of the flow in the step region is a linear (i.e. small) perturbation of the two-dimensional base flow. A comparison of the present simulation results with experimental data shows close agreement concerning, for example, the flow topology in the step region, and the spanwise spacing of the characteristic streaks that form further downstream.

1. Introduction

Flow separation and recirculation caused by blunt obstacles or sudden constrictions in flow geometry play an important role in many engineering applications. Pipe systems, for example in chemical reactors or food-processing devices, often exhibit abrupt changes in tube diameter, or may be furnished with baffles or ribs that obstruct the flow path. Similarly, flows over and around wall-mounted obstacles or through orifices are frequently encountered in practice, examples being heat exchangers, combustors, or flow meters, to name but a few. The transport and mixing properties of such flows are therefore of great interest. A prototype configuration for studying separation ahead of blunt obstacles, which has received particular attention

† Author to whom correspondence should be addressed.

https://doi.org/10.1017/S0022112003004440 Published online by Cambridge University Press

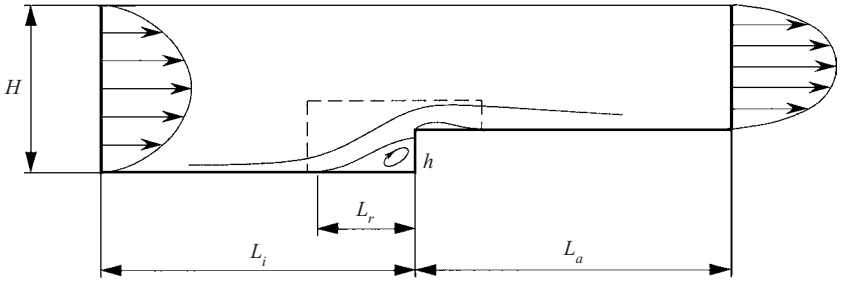


FIGURE 1. Sketch of two-dimensional forward-facing step flow in a plane channel. h and H denote the height of the step and the channel height in the oncoming stream, respectively. The flow separates ahead of the step and reattaches at the vertical wall. In general, the length L_r of the recirculation zone depends on the Reynolds number. Note that on top of the step, a second smaller separation bubble may develop. L_i denotes the distance of the inflow plane upstream of the step as employed in the simulations. L_a is the according distance between step and outflow plane. The dashed line indicates the region considered in the linear-stability analysis.

in the past, is the flow over a forward-facing step (FFS) in a plane channel (see e.g. Abu-Mulaweh, Armaly & Chen 1996*a*, *b*; Chiba, Ishida & Nakamura 1995; Pollard, Wakarani & Shaw 1996; Stüer, Gyr & Kinzelbach 1999). This generic flow problem will also be considered in the present work. Closely related configurations that were also studied include the forward-facing double step analysed by Shakouchi & Kajino (1993), flows along circular cylinders with a sudden increase in diameter (see Driver & Hebbar 1989; Watanabe & Kamiya 1996), or the flow over surface-mounted square ribs or cubes examined, for example, by Chou & Chao (2000), Dimaczek *et al.* (1989), and Werner & Wengle (1989).

Earlier work on the FFS configuration had focused on the purely two-dimensional case (see e.g. Dennis & Smith 1980; Mei & Plotkin 1986), which is sketched in figure 1. The key features of the flow are a recirculation zone with separation occurring ahead of the step, reattachment at the vertical wall, and another smaller separation zone downstream of the corner point. The simplification to two dimensions may seem natural at first sight, but it should be noted that many separated flows have a tendency towards three-dimensionality. This is reflected, for example, in the stability properties of separated boundary layers at high Reynolds numbers (Re), where three-dimensional modes may become preferentially excited as a consequence of non-parallelism of the base flow (Stewart & Smith 1987; see also the overview article Smith 2000 and the references cited therein). For forward-facing steps and similar configurations, experiments as well as numerical simulations clearly revealed that the separation zone ahead of the step develops a three-dimensional structure (see Chiba *et al.* 1995; Pollard *et al.* 1996; Smith & Walton 1998; Stüer *et al.* 1999; Chou & Chao 2000). Note, however, that this three-dimensionality not only occurs at high Reynolds numbers; it is also observed with flows at low Reynolds numbers down into the viscous regime.

Among the most comprehensive studies of FFS flow is the work of Stüer (1999) who performed experiments in a water channel for two different constrictions ($h/H = 1/4$ and $1/2$, respectively, see figure 1), and for Reynolds numbers as low as about 30. The three-dimensionality is recognized from his hydrogen-bubble visualizations which show the formation of streaky structures downstream of the step corner (see figure 2). Such streaks were also observed by Pollard *et al.* (1996), and they closely resemble

https://doi.org/10.1017/S0022112003004440 Published online by Cambridge University Press

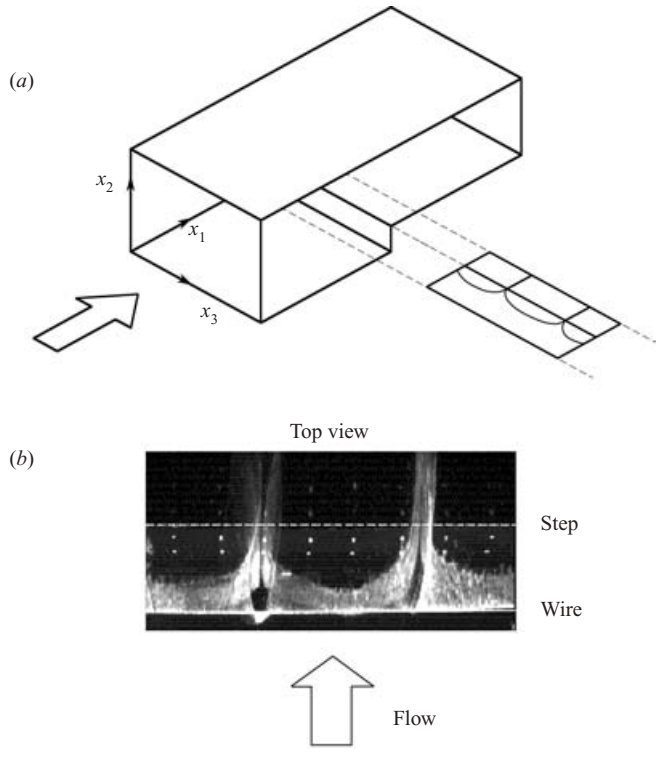


FIGURE 2. Hydrogen-bubble visualization of Stüer (1999), showing the formation of streaky structures downstream of the step. The hydrogen bubbles are generated from electrical pulses through a thin wire placed in the oncoming stream. (*a*) illustrates the location of the region depicted in (*b*). The Reynolds number of the flow is $Re = 330$.

the structures that Chou & Chao (2000) report from their experiments on flows over rib-like obstacles. In addition, Stüer's detailed velocity measurements show the three-dimensional flow ahead of the step to be an open-type separation rather than a closed separation as encountered in two dimensions. The streamline pattern computed from his experimental data reveal contracting spiralling motions in the separation zone, which resemble the flow structures ahead of three-dimensional blunt obstacles described by Smith & Walton (1998). A simplified sketch of this flow pattern at the step is provided in figure 3, which illustrates how fluid entrained into the separation region is transported in the spanwise direction, before being released over the step corner. The spanwise positions where the entrained fluid is released coincide with the locations of streak formation seen in figure 2.

Much has been learned in recent years about the topology of laminar FFS flow at low Reynolds numbers, but still little is known about why a stable and seemingly two-dimensional flow in the oncoming stream breaks up into a three-dimensional pattern at the step. Attempts to explain this phenomenon resorted to very diverse fluid-dynamics mechanisms. For example, Chiba *et al.* (1995) held a Görtler-type instability responsible for the onset of three-dimensionality, while other authors assumed that near-wall streaks in the oncoming flow may play a dominant role regarding the three-dimensional structure and the streak formation downstream (see Pollard *et al.* 1996). Such near-wall streaks are prominent features of wall turbulence (see Robinson 1991; Wilhelm, Härtel & Eckelmann 1998) and may be of importance in turbulent flows

https://doi.org/10.1017/S0022112003004440 Published online by Cambridge University Press

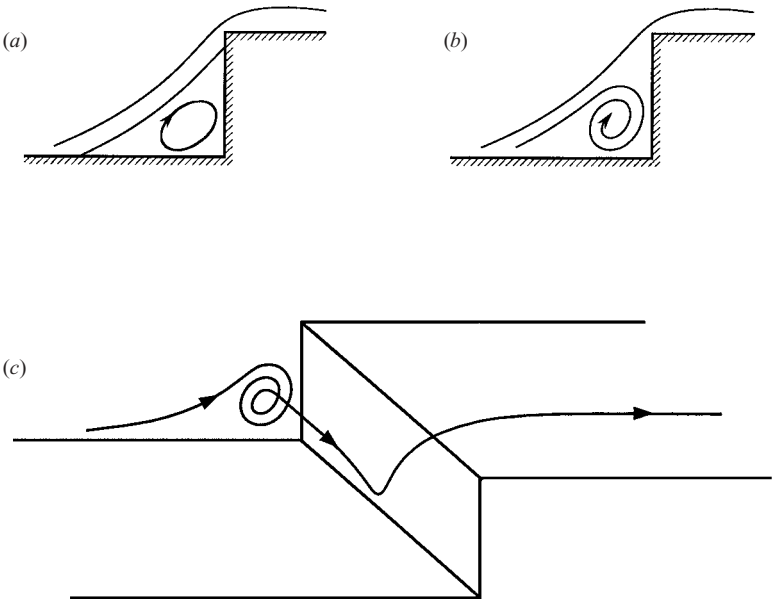


FIGURE 3. Sketch of the structure of the separation region in front of a forward-facing step. (*a*) Two-dimensional flow featuring a closed separation bubble. (*b*) Side view and (*c*) perspective view of the open recirculation zone typically encountered in three dimensions. The streamline in (*c*) illustrates how oncoming fluid is entrained into the separation zone and transported in the spanwise direction, before being released over the step corner.

at higher Reynolds numbers. However, in low-Reynolds-number flows such near-wall streaks do not exist. Finally, an absolute instability of the two-dimensional separation bubble itself has been suggested in the literature (see e.g. Stüer 1999), a mechanism that gains some plausibility from the omnipresence of the three-dimensional structure in a wide variety of configurations.

To further improve the understanding of FFS flow, and to shed more light on the conditions on which the two-dimensional–three-dimensional transition at the step depends, we have undertaken a computational analysis where the response of a two-dimensional flow to three-dimensional disturbances is studied in a highly controlled setting. In this analysis, we are especially interested in lower Reynolds numbers where the oncoming flow far ahead of the step is stable to all disturbances. Results will be presented here for a Reynolds number of $Re = 330$, based on the step height and bulk velocity. Moreover, we only consider the case of a step which is infinitely extended in the spanwise direction, meaning that potential boundary effects arising from a finite width of the step are not taken into account. However, available experimental evidence suggests that boundary effects do not play a key role in the present case, at least as far as the structure of the separation zone is concerned. For example, Stüer (1999) systematically varied the end parts of his step configuration in the water tank, but did not observe any influence on the three-dimensional flow pattern in the separation region.

The present study comprises a linear-stability analysis of the two-dimensional flow in the step region as well as three-dimensional direct numerical simulations. Among the issues we seek to clarify is whether or not a two-dimensional separation bubble ahead of a step is absolutely unstable (in the sense of Huerre & Monkewitz 1990), i.e. whether a weak three-dimensionality of the recirculation region itself may grow

https://doi.org/10.1017/S0022112003004440 Published online by Cambridge University Press

to large amplitudes even if the oncoming flow is undisturbed. Moreover, we will consider in detail the role that inflow disturbances play for the two-dimensional–three-dimensional transition at the step. Since high accuracy is required in any computational analysis of hydrodynamic stability problems, a numerical method based on spectral and spectral-element discretization is employed in the simulations. The main features of this numerical technique are briefly outlined in § 2 where the governing equations are also presented. Section 3 then contains results from the linear-stability analysis of the flow in which only a small subdomain of the channel enclosing the step is considered. This stability analysis is based on two-dimensional simulation data and employs a wave ansatz for the three-dimensional disturbances. The main part of the paper, § 4, is then devoted to the simulation results where the evolution of disturbances of various types and amplitudes in the flow are studied in detail. Finally, § 5 summarizes the main findings of our study.

2. Governing equations and simulation approach

We are concerned with incompressible flows of Newtonian fluids in a plane channel containing a forward-facing step of height h. The flow domain is sketched in figures 1 and 2, where H is the channel height in the oncoming flow, and x_1, x_2 and x_3 denote the streamwise, wall-normal and spanwise directions of the flow domain, respectively. The ratio of step height to channel height h/H is generally set to 1/4 here. In the simulations, the flow domain is bounded by inflow and outflow planes located at distances of L_i and L_a, respectively, from the step. Since the position of these inflow/outflow planes may exert an influence on the solution, we performed two-dimensional calculations in which L_i and L_a were varied systematically. From these simulations, we found that the finite size of the flow domain has a negligible effect on the flow field in the neighbourhood of the step provided that at least $L_i = 20$ and $L_a = 30$. These values of L_i and L_a were then used in all simulations. At the open boundaries in the spanwise direction, we assume the flow to be periodic (note that in experiments the structure of the three-dimensional separation region typically appears as a quasi-periodic cellular pattern). Finally, solid boundaries are imposed at the bottom and top of the channel, as well as at the vertical step wall.

The fluid motion in the present case is governed by the incompressible Navier–Stokes equations. Using the bulk velocity U_Q of the flow ahead of the step (defined as the volume flux divided by the channel cross-section) and the step height h for normalization, these equations read in dimensionless form

$$\frac{\partial \boldsymbol{u}}{\partial t} - \frac{1}{Re}\Delta \boldsymbol{u} + \nabla q = -\mathscr{C}(\boldsymbol{u})\,\boldsymbol{u}, \tag{1}$$

$$\operatorname{div} \boldsymbol{u} = 0, \tag{2}$$

where $\boldsymbol{u}$ denotes the velocity and $\mathscr{C}(\boldsymbol{u})\,\boldsymbol{u}$ the nonlinear term. The term q is the pressure divided by the density (which is assumed constant). In equation (1), $Re = U_Q h/\nu$ is the Reynolds number of the flow which is computed from U_Q, h and the kinematic viscosity ν of the fluid. As boundary conditions in the inflow plane, we prescribe developed channel flow with a parabolic velocity profile which can be written in non-dimensional form as

$$u_1(x_2) = \tfrac{3}{2}x_2(1 - x_2/4). \tag{3}$$

In some of the simulations, three-dimensional disturbances of various shape and amplitude are superimposed to the Poiseuille parabola at inflow. In the outflow

https://doi.org/10.1017/S0022112003004440 Published online by Cambridge University Press

plane, homogeneous Neumann conditions are used for all three velocities, meaning that the respective gradients in x_1 have to vanish. Numerical tests showed that with this boundary condition no undesired feedback effects occurred from the outflow boundary on the flow in the interior of the domain.

To solve the basic equations numerically, a spatial discretization is performed which uses a Fourier scheme in the homogeneous spanwise direction x_3, i.e.

$$\boldsymbol{u}(\boldsymbol{x},t) = \sum_{m=-N_z/2+1}^{N_z/2-1} \hat{\boldsymbol{u}}^m(x_1,x_2,t)\exp(\mathrm{i}\,m\alpha_0 x_3), \tag{4}$$

$$q(\boldsymbol{x},t) = \sum_{m=-N_z/2+1}^{N_z/2-1} \hat{q}^m(x_1,x_2,t)\exp(\mathrm{i}\,m\alpha_0 x_3), \tag{5}$$

where $\hat{\boldsymbol{u}} = (\hat{u}_1, \hat{u}_2, \hat{u}_3)$ and $\hat{q}$ are the complex Fourier coefficients (modes) of velocity and pressure, respectively. $\alpha_0 = 2\pi/L_z$ denotes the fundamental wavenumber in the spanwise direction (L_z being the length of periodicity), and $\mathrm{i} = \sqrt{-1}$. Inserting the Fourier expansions of order N_z for the velocities $\boldsymbol{u}$ and the pressure q into the governing equations and applying the standard Galerkin procedure yields a system of four coupled equations for each of the N_z Fourier components

$$\frac{\partial \hat{\boldsymbol{u}}^m}{\partial t} - \frac{1}{Re}\left(\frac{\partial^2}{\partial x_1^2} + \frac{\partial^2}{\partial x_2^2} - m^2\alpha_0^2\right)\hat{\boldsymbol{u}}^m + \hat{\nabla}\hat{q} = -\hat{\mathscr{C}}^m(\hat{\boldsymbol{u}}^m)\,\hat{\boldsymbol{u}}^m, \tag{6}$$

$$\left(\frac{\partial}{\partial x_1} + \frac{\partial}{\partial x_2} + \mathrm{i}\,m\alpha_0\right)\hat{\boldsymbol{u}}^m = 0, \tag{7}$$

where the term on the right-hand side of equation (6) denotes the Fourier transform of the nonlinear term, and

$$\hat{\nabla} = (\partial/\partial x_1, \partial/\partial x_2, \mathrm{i}\,m\alpha_0)^T. \tag{8}$$

The above equations are then discretized in the two inhomogeneous directions by a spectral-element method (SEM) which decomposes the (x_1, x_2)-plane into a number of K non-overlapping subdomains (spectral elements). In each element, the solutions for velocity and pressure are expanded in tensor-product-based polynomials of order N and $N-2$, respectively. While the velocities are discretized at the Gauss–Lobatto–Legendre points, the pressure is discretized at the Gauss–Legendre points. Detailed discussions of this so-called $P_N - P_{N-2}$ SEM can be found, for example, in Maday & Patera (1989), Fischer (1997) or Wilhelm (2000). As an aside, we remark that the formulation of the nonlinear term $\mathscr{C}(\boldsymbol{u})\,\boldsymbol{u}$ requires care in this type of spectral-element approach, as some of the more widely used forms are prone to a numerical instability (see Wilhelm & Kleiser 2000, 2001). Here, we use the nonlinear term in the so-called convective form defined by

$$\mathscr{C}(\boldsymbol{u})\,\boldsymbol{u} = (\boldsymbol{u}\cdot\nabla)\boldsymbol{u}. \tag{9}$$

Finally, the time discretization of the governing equations is accomplished by a semi-implicit method, with the linear terms being treated implicitly using a second-order backward-differentiation scheme, and the nonlinear terms being treated explicitly by a second-order extrapolation method (cf. Karniadakis, Israeli & Orszag 1991).

The specific advantage of a spectral-element discretization is that it allows us to combine high numerical accuracy with flexibility concerning the distribution of mesh points. This flexibility is needed to cope with the flow in the vicinity of the step corner

https://doi.org/10.1017/S0022112003004440 Published online by Cambridge University Press

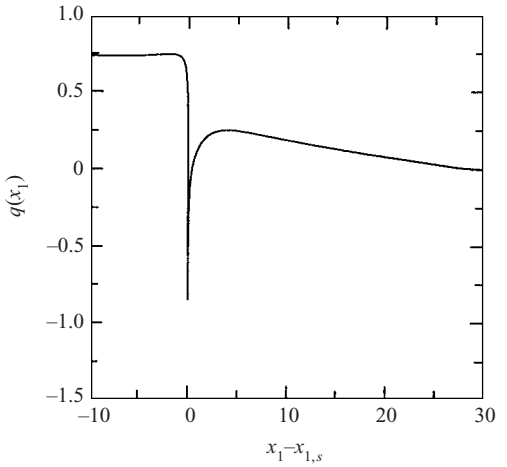


FIGURE 4. Pressure q at height $x_2 = h + \delta x_2$ as a function of the relative distance from the step corner located at $x_{1,s}$. δx_2 is the wall distance of the first grid line of the pressure mesh in the downstream section of the channel. Result for two-dimensional FFS flow at $Re = 330$ (Wilhelm & Kleiser 2001).

where steep gradients occur in vorticity and pressure (see e.g. Dennis & Smith 1980). To illustrate this more clearly, figure 4 gives the pressure distribution along a grid line immediately above the corner point, as obtained from a two-dimensional simulation for $Re = 330$ by Wilhelm & Kleiser (2001). To achieve good resolution in this part of the flow domain, we employ the 'geometric mesh refinement' strategy proposed by Gerdes & Schötzau (1999), in which the size of the spectral elements decreases with decreasing distance from the corner. The structure of the resulting mesh in the (x_1, x_2)-plane, as it is generally used in the present study, can be seen from figure 5. Note that mesh refinement is applied in both directions x_1 and x_2.

3. Linear stability analysis

Before discussing the numerical simulations in more detail in § 4, we will present a linear stability analysis, which we performed in order to clarify whether a purely two-dimensional separation bubble ahead of a (infinitely extended) step is prone to some three-dimensional absolute instability. In this analysis, we concentrate on a small subdomain of the flow enclosing the separation zone and the step corner, as indicated in figure 1. As a basis for the stability study, a highly-resolved two-dimensional base flow is taken from the simulations of Wilhelm & Kleiser (2002). The topology of the two-dimensional base flow is illustrated in figure 6 by means of streamlines. Both the recirculation bubble in front of the step and a separation zone downstream of the corner are clearly visible. The approach we have taken for the stability analysis is essentially the same as that employed by Härtel, Carlsson & Thunblom (2000) and Graf, Meiburg & Härtel (2002), who investigated three-dimensional absolute instabilities in natural convection flows and Hele-Shaw flows, respectively. For this reason, we will give only a brief discussion of the main aspects of the method here. Note also that our approach is very similar to the techniques employed previously by other authors studying three-dimensional instabilities in separated flows (see Kaiktsis, Karniadakis & Orszag 1991, for backward-facing step flow, or Theofilis, Hein & Dallmann 2000, for a study of two-dimensional separation bubbles).

https://doi.org/10.1017/S0022112003004440 Published online by Cambridge University Press

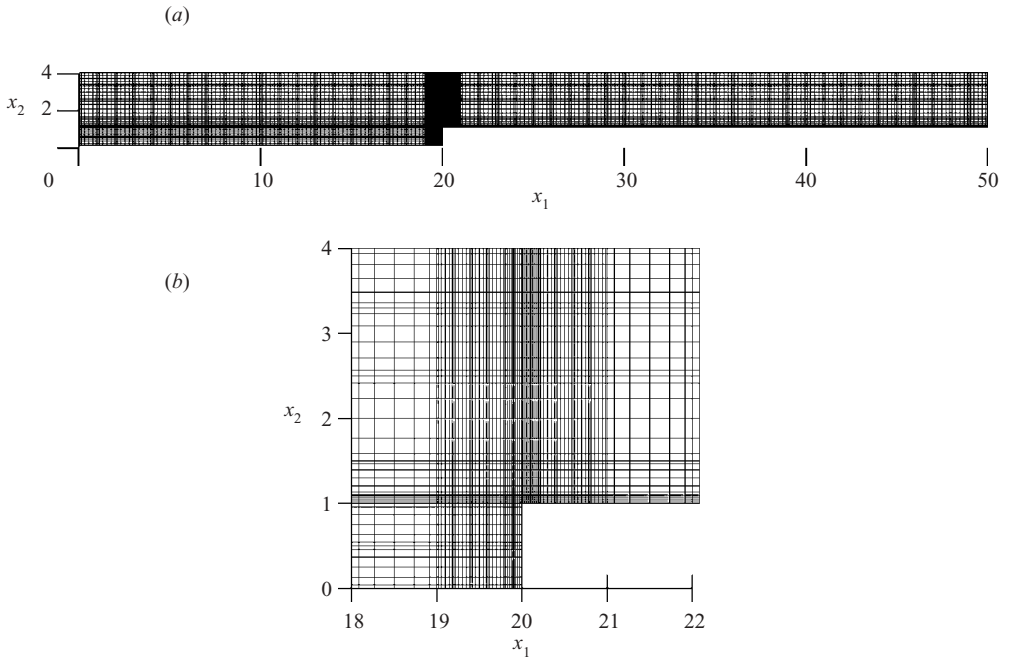


FIGURE 5. Computational grid with mesh refinement towards the step corner. In the region to the left of the step (i.e. in the Cartesian region $[0, 20] \times [0, 4]$), $26 \times 12 = 312$ spectral elements are used. The region to the right ($[20, 50] \times [1, 4]$) is discretized by $36 \times 7 = 252$ elements. The polynomial order within each element is $N = 6$. (*b*) shows an enlargement of the step region.

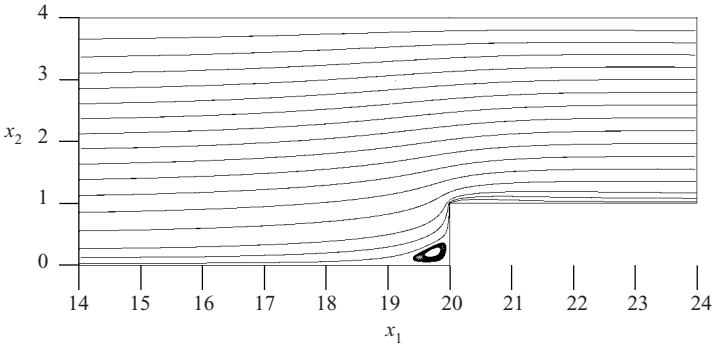


FIGURE 6. Streamlines of two-dimensional FFS flow at $Re = 330$.

As usual in linear stability studies (see Drazin & Reid 1981), we set out from a decomposition of all flow quantities into a basic part and a (infinitesimally) small disturbance. While the base flow is two-dimensional, the disturbance is assumed to be three-dimensional. Indicating the mean flow by an overbar and the disturbance by a prime, this decomposition reads

$$\boldsymbol{u}(\boldsymbol{x}, t) = \overline{\boldsymbol{u}}(x_1, x_2) + \boldsymbol{u}'(x_1, x_2, x_3, t), \tag{10}$$

$$q(\underline{x}, t) = \overline{q}(x_1, x_2) + q'(x_1, x_2, x_3, t). \tag{11}$$

For the disturbance, we employ an ansatz which is wavelike in the spanwise direction (wavenumber α), and which is stationary in that it does not travel in the spanwise

https://doi.org/10.1017/S0022112003004440 Published online by Cambridge University Press

direction. Finally, assuming the dominant mode to grow (or decay) exponentially with time at a rate σ, the disturbances can be written in the following form

$$f' = \hat{f}(x_1, x_2)\cos(\alpha x_3)\,\mathrm{e}^{\sigma t} \quad \text{for} \quad f' = u_1', u_2', q', \tag{12}$$

$$f' = \hat{f}(x_1, x_2)\sin(\alpha x_3)\,\mathrm{e}^{\sigma t} \quad \text{for} \quad f' = u_3', \tag{13}$$

where $\hat{f}$ is the amplitude function (or shape function) that does not depend on time. The evolution equations for the perturbations are obtained by inserting (10)–(13) into the basic equations (1) and (2), and subtracting the equations for the mean flow. Upon linearization, we then obtain the stability equations

$$\frac{\partial \hat{u}_1}{\partial x_1} + \frac{\partial \hat{u}_2}{\partial x_2} + \alpha \hat{u}_3 = 0, \tag{14}$$

$$\sigma \hat{u}_1 + \hat{u}_1 \frac{\partial \bar{u}_1}{\partial x_1} + \hat{u}_2 \frac{\partial \overline{u}_1}{\partial x_2} + \overline{u}_1 \frac{\partial \hat{u}_1}{\partial x_1} + \bar{u}_2 \frac{\partial \hat{u}_1}{\partial x_2} + \frac{\partial \hat{q}}{\partial x_1} = \frac{1}{Re}\left(\frac{\partial^2}{\partial x_1^2} + \frac{\partial^2}{\partial x_2^2} - \alpha^2\right)\hat{u}_1, \tag{15}$$

$$\sigma \hat{u}_2 + \hat{u}_1 \frac{\partial \bar{u}_2}{\partial x_1} + \hat{u}_2 \frac{\partial \bar{u}_2}{\partial x_2} + \bar{u}_1 \frac{\partial \hat{u}_2}{\partial x_1} + \bar{u}_2 \frac{\partial \hat{u}_2}{\partial x_2} + \frac{\partial \hat{q}}{\partial x_2} = \frac{1}{Re}\left(\frac{\partial^2}{\partial x_1^2} + \frac{\partial^2}{\partial x_2^2} - \alpha^2\right)\hat{u}_2, \tag{16}$$

$$\sigma \hat{u}_3 + \bar{u}_1 \frac{\partial \hat{u}_3}{\partial x_1} + \overline{u}_2 \frac{\partial \hat{u}_3}{\partial x_2} - \alpha \hat{q} = \frac{1}{Re}\left(\frac{\partial^2}{\partial x_1^2} + \frac{\partial^2}{\partial x_2^2} - \alpha^2\right)\hat{u}_3. \tag{17}$$

The system (14)–(17) constitutes an eigenvalue problem for the temporal growth rate σ which depends on the given two-dimensional base flow $\overline{\boldsymbol{u}}$, on the wavenumber α, and on Re. This eigenvalue problem is solved numerically by discretizing all spatial derivatives using a spectral-element collocation technique on a mesh with N nodal points. This mesh is – in the subdomain considered – very similar to the grid used for the base flow. These meshes are not identical because a slightly higher order of discretization was needed in the stability analysis in order to reduce the total number of nodal points. To obtain the mean-flow velocities on this mesh, cubic spline interpolation was employed.

The spatial discretization transforms the stability equations into a general algebraic eigenvalue relation involving two $N \times N$ matrices which contain the coefficients of the differentiation schemes and the coupling terms between the discretized stability equations. The number N of nodal points depends on the extent of the subdomain and the computational resolution employed. In the present study, about 10^3 nodal points were used, meaning that the matrices consist of some 10^6 elements each. To complete the mathematical formulation, boundary conditions for the perturbations must be prescribed. At the solid walls, homogeneous Dirichlet conditions are appropriate, but at the open boundaries of the subdomain no natural boundary conditions are available. However, in general we observed the eigenvalues to be very little sensitive to the boundary conditions, and therefore homogeneous Dirichlet conditions were prescribed at the open boundaries too. With the boundary conditions implemented, the discretized system was then solved for the leading eigenvalues, using an iterative procedure based on the implicitly restarted Arnoldi method (see Sorensen 1992).

The result of the stability analysis, i.e. the stability diagram of the flow, is depicted in figure 7 where the amplification rate σ of the least-damped mode is given as a function of the spanwise wavenumber α. The range in α examined extends from 0.1 to 20, but in the figure only the region around the maximum is shown. Given

https://doi.org/10.1017/S0022112003004440 Published online by Cambridge University Press

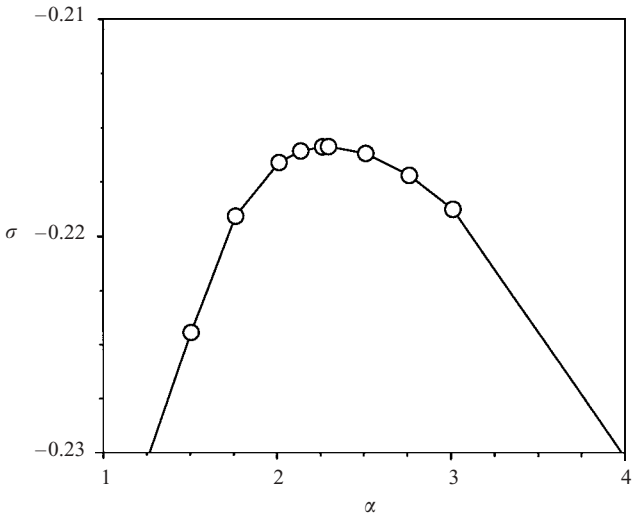


FIGURE 7. Linear-stability diagram of the flow in the step region. Shown is the amplification rate σ of small disturbances as function of the spanwise wavenumber α.

that all eigenvalues are negative, it is clear that according to our investigation an absolute instability of the two-dimensional flow in the step region does not exist for the parameters considered. Rather, disturbances in this region will quickly be damped out, making the flow return to an unperturbed two-dimensional state. The stability results displayed in figure 7 are valid for small disturbances only, but in the subsequent section we will give evidence that large-amplitude three-dimensional perturbations in the separation region do decay as well. An interesting observation from figure 7 is that the pronounced maximum of the stability curve indicates the existence of some preferred (least-damped) spanwise length scale of the flow at the step. The maximum of the stability curve is located at about $\alpha = 2.1$ which corresponds to a spanwise wavelength of three times the step height. This agrees closely with the typical spacing of three-dimensional structures observed in experiments.

From figure 7 it is furthermore seen that the damping becomes stronger with increasing two-dimensionality (i.e. $\alpha \to 0$). A similar dominance of three-dimensional modes over two-dimensional ones is known from separated flows at high Reynolds number (Stewart & Smith 1987), where three-dimensional modes are preferentially amplified when the separation angle is sufficiently strong.

4. Numerical simulation results

The three-dimensional simulations performed in the present study were generally initialized with a developed two-dimensional solution and superimposed three-dimensional perturbations in the initial flow field or in the inflow boundary conditions. Unless stated otherwise, the length of periodicity in the spanwise direction was set to π ($\alpha_0 = 2$), i.e. to slightly more than three times the step height. This choice was motivated by the typical streak spacing observed in experiments. In total, 564 spectral elements with a polynomial degree of 6 were employed for the spatial discretization in the (x_1, x_2)-plane.

https://doi.org/10.1017/S0022112003004440 Published online by Cambridge University Press

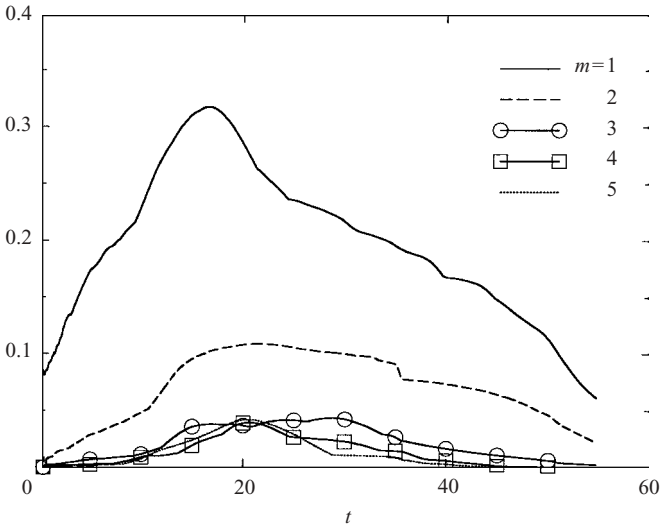


FIGURE 8. Time history of the maximum $|\hat{u}_1(x_1)|_{max}$ of the spanwise Fourier amplitudes of u_1. The simulation is started with random three-dimensional perturbations in the initial flow field superimposed onto a developed two-dimensional flow. As the inflow boundary condition, undisturbed Poiseuille flow is prescribed.

4.1. *Response to initial disturbances*

The first series of simulations performed was intended to complement the linear-stability analysis by studying the flow response to finite-amplitude random perturbations in the initial field. As inflow boundary conditions, however, undisturbed two-dimensional Poiseuille flows were prescribed in these runs. To make sure that potential linear as well as nonlinear mechanisms are captured, various initial disturbance amplitudes up to 10% (relative to the bulk velocity) were considered, and the development of three-dimensionality was monitored by the time history of the maximum Fourier amplitudes $|\hat{u}_1|_{max}$ of the streamwise velocity component over the (x_1, x_2)-plane. In agreement with the stability analysis, these simulations show that the perturbation amplitudes of the three-dimensional initial noise eventually decay, meaning that the flow returns to two-dimensionality. This is illustrated in figure 8 where the maximum $|\hat{u}_1(m, t)|_{max}$ of the Fourier components of the streamwise velocity is depicted as a function of time, i.e.

$$|\hat{u}_1(m, t)|_{max} := \max_{x_1, x_2} |\hat{u}_1(x_1, x_2, m, t)|. \tag{18}$$

We remark that we conducted similar simulations for Reynolds numbers up to about 600 and obtained essentially the same results as for the Reynolds number $Re = 330$ considered here.

Although the flow eventually returns to a two-dimensional state, a growth of disturbance amplitudes is seen during an initial transient period in figure 8. The reason for this growth is that disturbances were superimposed to the flow in the entire computational domain rather than in the separation region only. Consequently, the flow approaching the step is perturbed for a time interval ΔT which scales with the length L_i of the inflow section and a velocity scale characterizing the downstream convective transport. Taking for the latter the bulk velocity U_Q yields $\Delta T \approx L_i/U_Q = 20$, a result which compares well with the duration of the phase of

https://doi.org/10.1017/S0022112003004440 Published online by Cambridge University Press

growth seen in figure 8. This result already hints at the important role that incoming perturbations play for the three-dimensionality in the step region, an issue which we will concentrate on in the remainder.

4.2. *The role of inflow disturbances*

Since in the present case the recirculation zone at the step is not unstable *per se*, it is clear that the two-dimensional–three-dimensional transition must be a sensitive response of the flow at the step to perturbations in the oncoming stream. To examine the response of the flow at the step to such inflow disturbances, we conducted simulations with different perturbations superimposed to the parabolic mean flow in the inflow plane. Two types of disturbance were considered:

(i) *Perturbations in streamwise velocity*. Variations of u_1 in the inflow plane slightly modulate the spanwise vorticity component ω_3 and introduce wall-normal vorticity ω_2. Here, perturbations u_1' of the following form are used

$$u_1'(x_2, x_3) = \varepsilon_e \sin(2\,x_3)\, \sin(x_2\,\pi/2), \tag{19}$$

where ε_e is a parameter determining the disturbance level.

(ii) *Perturbations in streamwise vorticity ω_1 by longitudinal vortices.* Longitudinal vortices play an important role in numerous flows and may persist over long distances. In our simulations, such vortices were introduced by boundary conditions for the velocity components, which were taken from a Stokes' solution of decaying vortices in a fluid at rest between two parallel walls. As a measure ε_e for the disturbance amplitude, we have taken the maximum value of the spanwise velocity in the inflow plane.

As in the simulations discussed before, the steady-state two-dimensional solution was used for initializing the flow field. The flow evolution was then followed in time until stationarity was re-established throughout the flow domain. The unsteady transient typically lasts some 50–60 dimensionless time units. The disturbance amplitude in the inflow plane was set to $\varepsilon_e = 0.05$, and 10 Fourier modes were used for the spatial discretization in x_3. This turned out to be sufficient to achieve a decay in modal energy of six orders of magnitude throughout the computation.

The flow field obtained with inflow perturbations in u_1 is visualized in figures 9 and 10, where sectional streamlines in the (x_2, x_3)-plane are depicted at five selected downstream positions. To improve visibility, two periods in the spanwise direction are shown. Note that, since u_2 and u_3 are not excited in the inflow plane, sectional streamlines cannot possibly be plotted at $x_1 = 0$, which is the reason why, in figure 9, the first cross-section shown is slightly offset from the entrance plane. Among the characteristic flow features recognized from the sectional streamlines is the formation of one stagnation point per period at the vertical wall. Moreover, a pair of counter-rotating vortices is seen which forms behind the step, and which persists for a long distance downstream. These vortices are intimately related to the streaks in the outflow part of the channel.

The second type of disturbances discussed above generates essentially identical flow structures at the step and further downstream. The respective graphs are not shown here for brevity, but can be found in Wilhelm (2000). This agreement makes clear that the flow features in the step region are largely independent of the kind of inflow disturbances imposed. Details of the background disturbances in the oncoming flow are of minor importance, therefore, for the evolution of the three-dimensionality at the step. This is also confirmed by simulations we conducted using random noise superimposed onto all velocity components in the inflow profile. Note that such a

https://doi.org/10.1017/S0022112003004440 Published online by Cambridge University Press

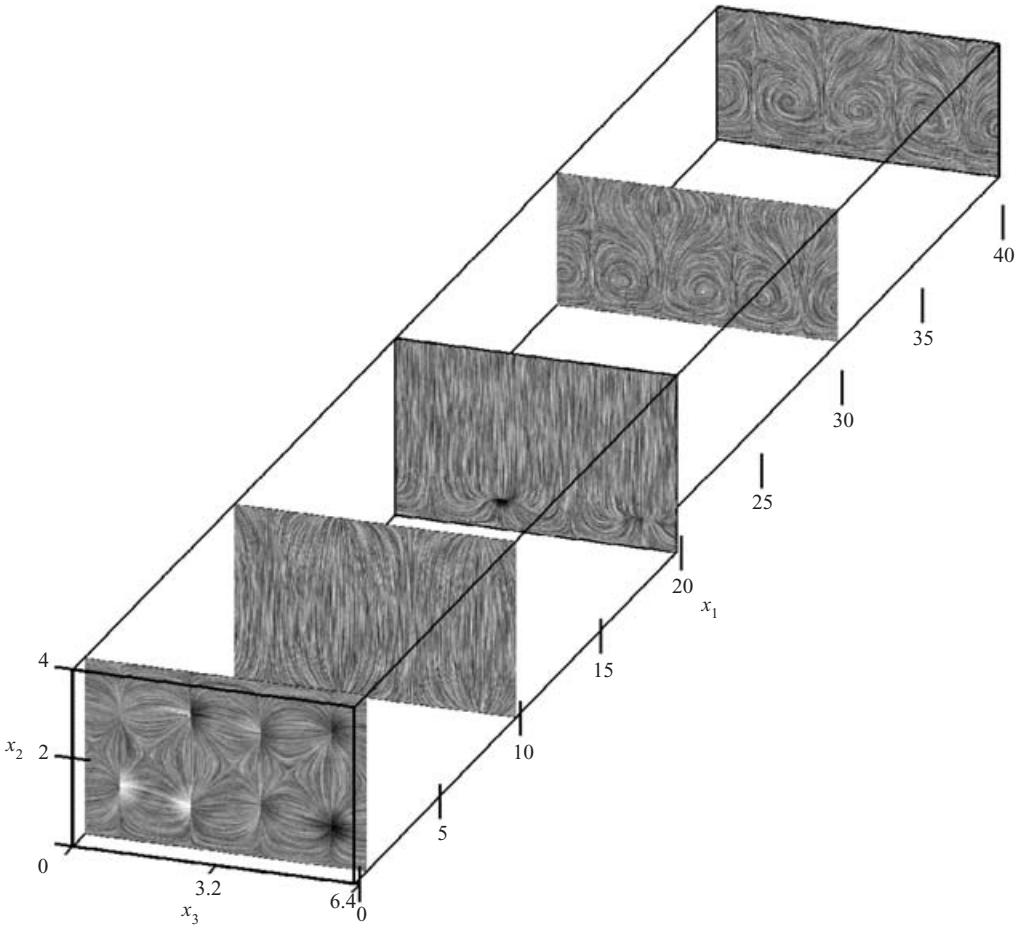


FIGURE 9. Sectional streamlines in (x_2, x_3)-planes at selected downstream positions. As inflow disturbance, perturbations in u_1 only are prescribed.

perturbation fundamentally differs from the other two in that it does not prescribe a dominant length scale from the outset. However, the results we obtained were again similar to those found in the other cases (see Wilhelm 2000).

4.3. *Flow structure at the step*

The formation of vortex pairs at the step goes along with a cellular structure of the separation region which is illustrated by means of wall-friction lines in figure 11. The boundary of separation is indicated by regions of convergent wall-friction lines. The principle sketch provided in the same figure indicates that the separation line extends up to the vertical wall of the channel. The point where the separation line meets the wall is located between two counter-rotating vortices in the downstream section, which is also the position where the fluid entrained into the separation region is released over the step. A good impression of the three-dimensional motion associated with the open separation can be achieved by following the trajectories of individual fluid elements in the step region. A side view and top view of such streamlines are given in figure 12. Starting points for the integration were placed in a cross-sectional area about 5.5 units in front of the step. It is seen from the figure how fluid is entrained into the vortex at the step, then moves either side in a spiralling motion, and finally, upon

https://doi.org/10.1017/S0022112003004440 Published online by Cambridge University Press

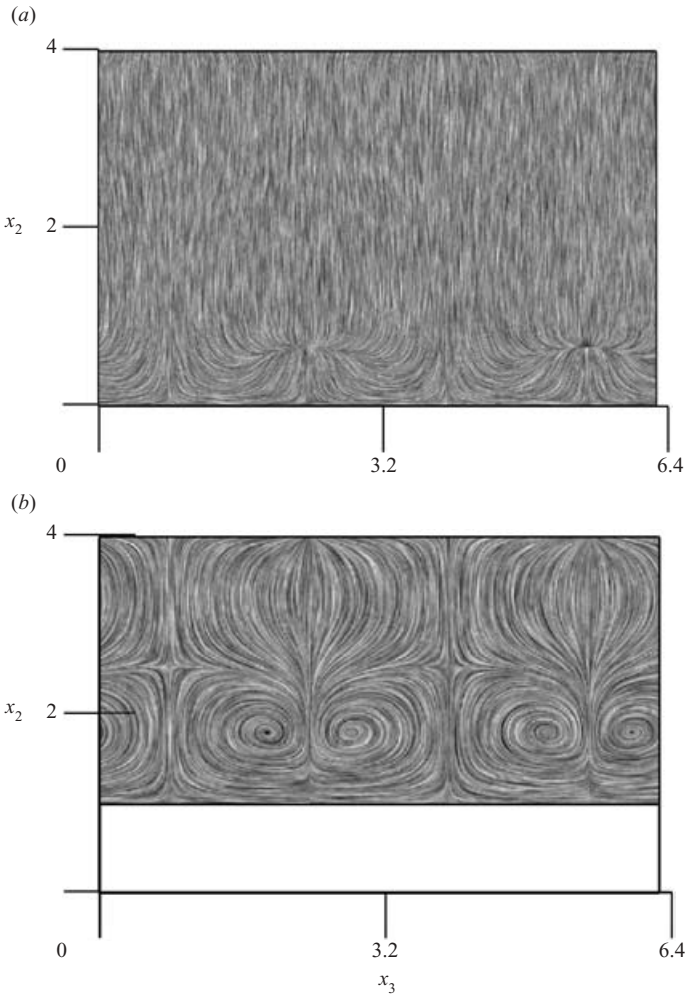


FIGURE 10. Sectional streamlines in (x_2, x_3)-planes at two selected downstream positions: (*a*) $x_1 = 20$ (step edge), (*b*) $x_1 = 30$. Same flow as in figure 9.

release from the separation region, flows over the step corner in two concentrated streaks. If the spanwise position of the streaks is compared with the position of the vortical structures in figure 10(*b*), it is seen that a pair of counter-rotating vortices is located between each two streaks. A direct comparison of the streamlines in figure 12 with streamlines obtained in experiments of Stüer *et al.* (1999) is provided in figure 13 where an excellent agreement is observed. Note that because of a slight non-stationarity in the experiments, particles starting from the same spatial location may follow different trajectories. However, such unsteadiness does not appear to be an essential feature of the flow at the step, and in our simulations we obtained strictly steady-state flow fields provided that the inflow disturbances were not varied with time.

The difference in flow topology between two-dimensional forward-facing step flow and the three-dimensional flow shown in figure 13 is pronounced, but it must be emphasized that the amplitude of the spanwise velocity component is still small in comparison to the maxima of the streamwise and normal velocities at the step. It is

https://doi.org/10.1017/S0022112003004440 Published online by Cambridge University Press

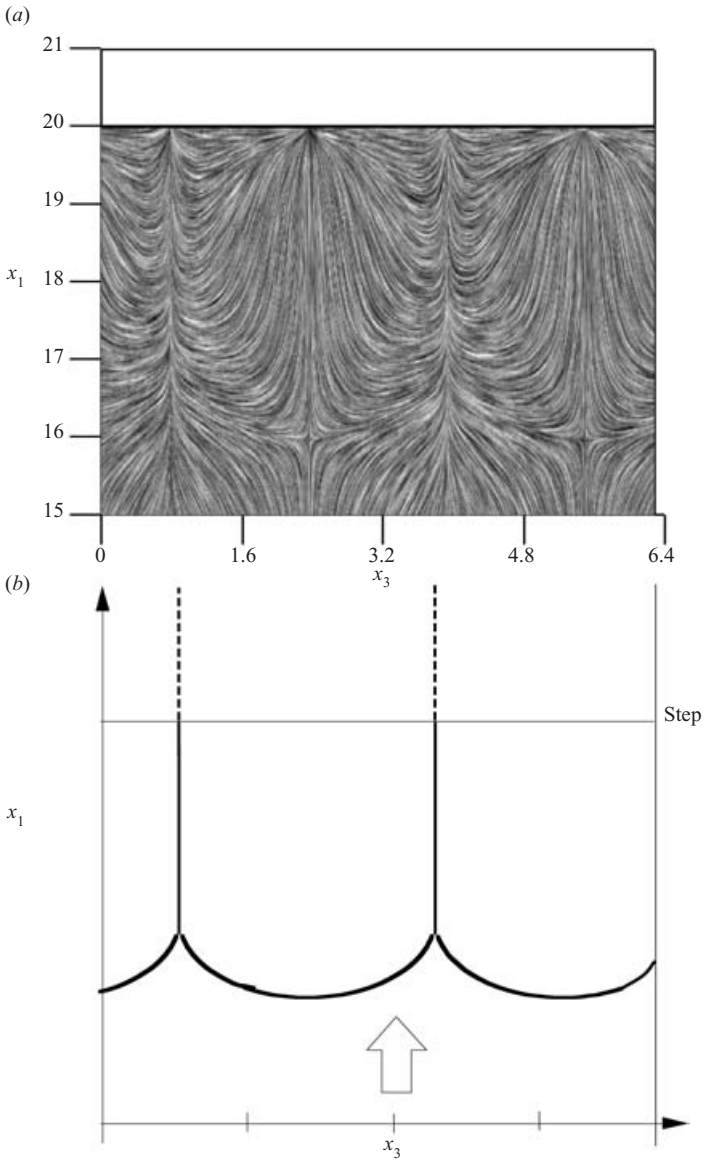


FIGURE 11. Wall-friction lines on the channel floor ahead of the step. Results for a disturbance amplitude of $\varepsilon_e = 0.05$ in the inflow plane (same flow as in figure 9). (*b*) shows the shape of the separation line (solid lines) and indicates the location of the streaks downstream of the step (dashed lines).

of interest, therefore, to compare the spanwise averaged three-dimensional flow field with the two-dimensional result, in order to assess to what extent the mean flow is distorted by the three-dimensionality in the separation region. Such a comparison is furnished in figure 14, which gives isocontours of the streamwise velocities u_1 and $\overline{u}_1$, respectively. Here, the overbar indicates a spanwise average, that is

$$\overline{u}_1 := \frac{1}{L_z} \int_0^{L_z} u_1 \, \mathrm{d}x_3.$$

https://doi.org/10.1017/S0022112003004440 Published online by Cambridge University Press

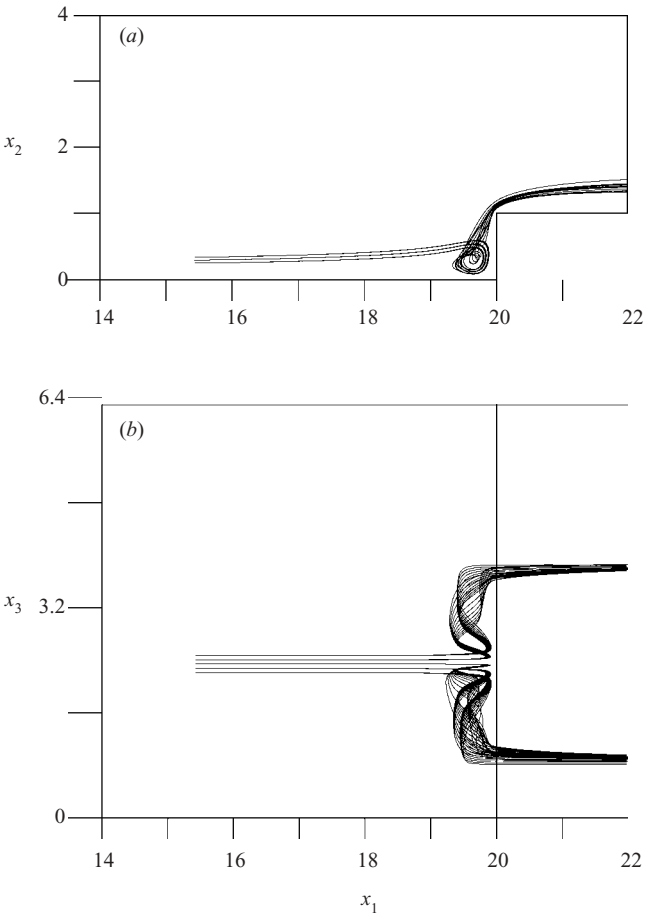


FIGURE 12. (*a*) Side view and (*b*) top view of streamlines in the step region. For the integration of the streamlines, the flow domain has been extended in the spanwise direction by one period. Same flow as in figure 9.

As seen from figure 14, the difference between the two-dimensional field and the averaged three-dimensional field is marginal, making clear that the break-up of the separation region at the step is only a weak perturbation to the two-dimensional base flow. In the following section we will address this point in a more quantitative fashion, and we will show that the three-dimensional perturbation is not only weak, but also of an inherently linear nature.

We wish to come back here briefly to the necessity of inflow disturbances for maintaining a three-dimensional flow. It has been demonstrated already that the flow is not absolutely unstable, and that random initial perturbations are convected out of the flow domain without causing a persisting two-dimensional–three-dimensional transition (see figure 8). This return to two-dimensionality occurs in the same fashion even if a fully developed three-dimensional structure already exists, meaning that the flow does not lock into a three-dimensional state that remains self-sustained in the absence of inflow disturbances. Using the converged stationary flow at time $t = 70$ as the initial condition, we continued the simulation for another 100 dimensionless time units, but without superimposed perturbations in the inflow plane. The response

https://doi.org/10.1017/S0022112003004440 Published online by Cambridge University Press

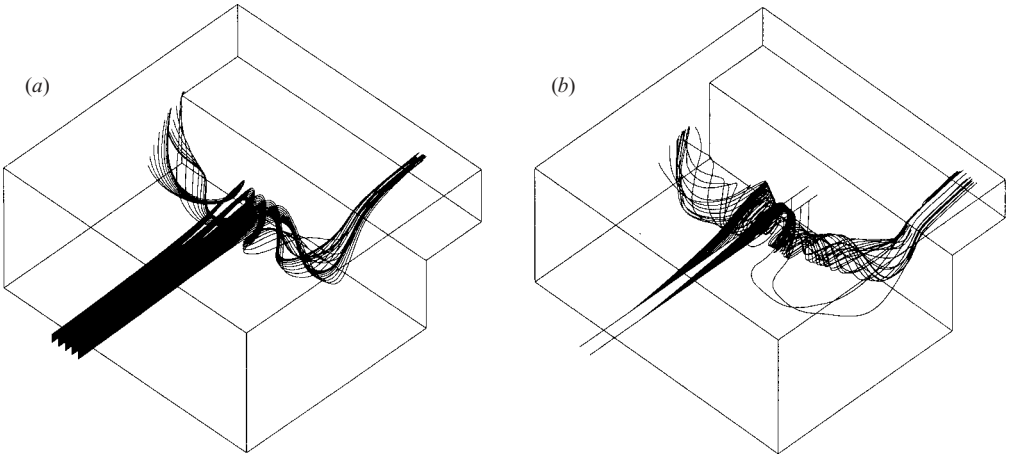


FIGURE 13. Perspective view of streamlines in the step region of FFS flow. Comparison of (*a*) simulation results (same flow as in figure 9) and (*b*) streamlines computed by Stüer (1999) from his experimental data. Note that only part of the flow domain in the normal direction is shown.

of the flow is illustrated in figure 15 where again the maximum $|\hat{u}_1(m,t)|_{max}$ of the Fourier components of the streamwise velocity is depicted as a function of time (see equation (18)). The maximum amplitude in the steady-state field at $t=70$ amounts to some 7% of U_Q for the fundamental mode ($m=1$), and slightly less for the higher harmonics. However, once inflow perturbations are no longer maintained, all disturbance amplitudes quickly decay indicating the return of the flow to the two-dimensional base state. At the end of the simulation, the maxima of all modes have dropped below 10^{-5}.

4.4. *Dependence on inflow disturbance amplitude*

Given the intimate relation between inflow disturbances and the three-dimensional break-up of the separation bubble, the intensity of the flow response at the step has to scale with the intensity of the perturbations in the oncoming flow. Moreover, since the feedback effect of the three-dimensional perturbations on the two-dimensional base flow was found to be marginal, we expect a linear scaling, with perturbation amplitudes at the step being proportional to perturbation amplitudes in the inflow plane. To examine this point, we conducted two further simulations with inflow conditions according to equation (19), but with disturbance levels of $\varepsilon_e=0.01$, and $\varepsilon_e=0.005$, respectively. As a measure of the three-dimensionality, a root-mean-square value of u_1 is employed here, which is based on the local deviation of the (time-converged) three-dimensional flow field from the two-dimensional mean flow, i.e.

$$u_{1,rms}(x_1)=\left(\frac{1}{HL_z}\int_0^H\int_0^{L_z}(u_1-\overline{u}_1)^2\,\mathrm{d}x_3\,\mathrm{d}x_2\right)^{1/2}. \tag{20}$$

In equation (20), $\overline{u}_1$ again denotes the spanwise average of the streamwise velocity, which is almost identical to a purely two-dimensional flow for all disturbance amplitudes considered. The variation of the r.m.s.-values with x_1 is displayed in figure 16, where a sensitive reaction of the flow in the step region can be observed in all cases. A sharp local increase of $u_{1,rms}$ occurs around $x_1=20$ which contrasts with the continuous decay of the disturbance amplitudes in the inflow and outflow

https://doi.org/10.1017/S0022112003004440 Published online by Cambridge University Press

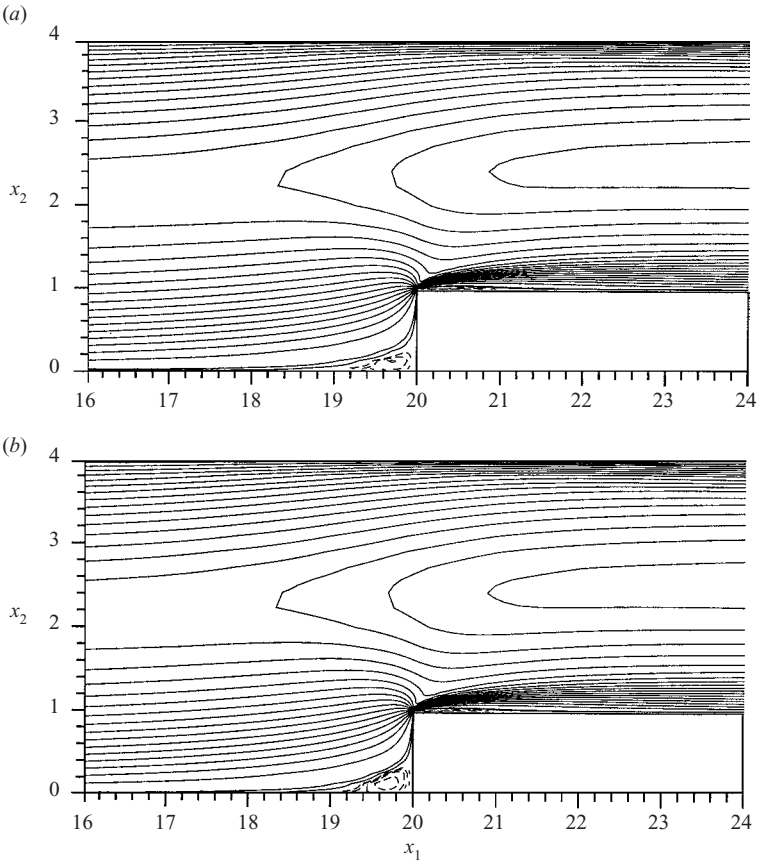


FIGURE 14. Comparison of two-dimensional and averaged three-dimensional FFS flow. (*a*) depicts isocontours of streamwise velocity u_1 as obtained from a two-dimensional simulation. (*b*) gives isolines of the spanwise-averaged velocity $\overline{u}_1$ from a three-dimensional simulation at the same Reynolds number. In the three-dimensional case, the disturbance amplitude in the inflow plane was set to $\varepsilon_e = 0.05$.

section of the channel. To make the linearity of the flow response at the step obvious, we have normalized all three curves in figure 16(*a*) by their values at the inflow location. The result is displayed figure 16(*b*), and it shows a perfect collapse of all curves as should be expected for a linear mechanism. This linearity is also seen from an inspection of the spatial shape of the dominant Fourier modes $\hat{u}_1(m = 1)$, which are depicted in figures 17 and 18 for the largest and smallest disturbance amplitude, respectively. In both cases, the shape function has been normalized by its maximum in the (x_1, x_2)-plane. Despite the fact that these maximum amplitudes differ by an order of magnitude, the shape functions are almost indistinguishable.

In addition to the shape function for $\hat{u}_1(m = 1)$, figure 17 also gives the associated shape functions for the other velocity components. From $\hat{u}_2$ and $\hat{u}_3$, the localization of the disturbance in the neighbourhood of the step is recognized very clearly. Larger disturbance levels exist only in the separation region and downstream of the corner, while the amplitudes quickly decay with increasing distance from the step. Perturbations in u_2 and u_3 become negligibly small beyond, say, $x_1 = 24$. Note that this is not in contradiction with the persistent vortex structures seen in the outflow

https://doi.org/10.1017/S0022112003004440 Published online by Cambridge University Press

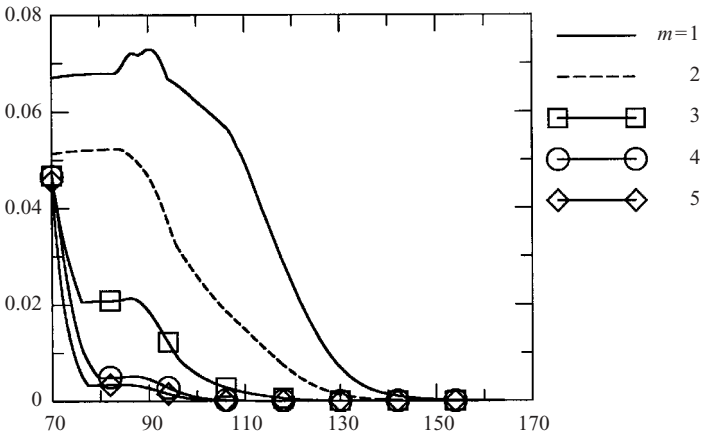


FIGURE 15. Development of three-dimensional modes in FFS flow after $t = 70$, when inflow disturbances are not maintained. Shown is the time history of the maximum $|\hat{u}_1|_{max}$ of the spanwise Fourier amplitudes of u_1. Results for Fourier modes $m = 1$–5.

section of the channel in figure 9. Since the sectional streamlines were computed from u_2 and u_3 only, they can reveal a weak vortical motion that could not easily be recognized from the pathlines of the fluid. Because u_1 is much larger here than the other two velocity components, particle trajectories are essentially straight lines in the outflow section of the channel.

A visual impression of how the three-dimensionality at the step gradually decreases with decreasing disturbance amplitudes can be gained from figure 19. In this figure, sectional wall-friction lines on the channel floor ahead of the step are shown for disturbance amplitudes of $\varepsilon_e = 0.01$ and $\varepsilon_e = 0.005$, respectively. Comparing these results with the result for $\varepsilon_e = 0.05$ in figure 19 illustrates that the spanwise distortion of the separation line weakens when the perturbation amplitude is reduced. For the smallest amplitude, the separation line varies almost sinusoidally without the sharp kinks, which are characteristic for larger disturbance levels. Clearly, for yet smaller perturbation amplitudes, the spanwise variation of the separation line diminishes further, but we found that the deformation of the separation line remains visible down to amplitudes as low as $\varepsilon = 10^{-4}$. This sensitivity of the shape of wall friction lines to minute disturbances highlights the difficulties that will be encountered when attempting to set up nearly two-dimensional FFS flows in the laboratory. Inflow disturbances well below 1% at some 10 step heights upstream of the step will be required.

To understand the substantial change in appearance of the flow in the separation region better, it is helpful to consider the wall friction of the flow from which the line of separation is defined. Figure 20 presents a comparison of the mean shear of the three-dimensional flow at the wall (which, again, is almost identical to the shear of the undisturbed two-dimensional solution), and the fluctuating component of the shear $\partial u_1/\partial x_2$ due to the dominant mode $m = 1$. The curves are given for a disturbance amplitude of $\varepsilon_e = 0.05$, but the results for the smaller disturbance amplitudes differ from the curves shown in figure 20 only with respect to the intensity of the fluctuating component $m = 1$. It is seen from the curves how the mean shear at the wall strongly decreases from its value of 1.5 in the undisturbed flow to values of the order of 0.1–0.2 ahead of the step. In this region, the amplitude of the fluctuating part takes its

https://doi.org/10.1017/S0022112003004440 Published online by Cambridge University Press

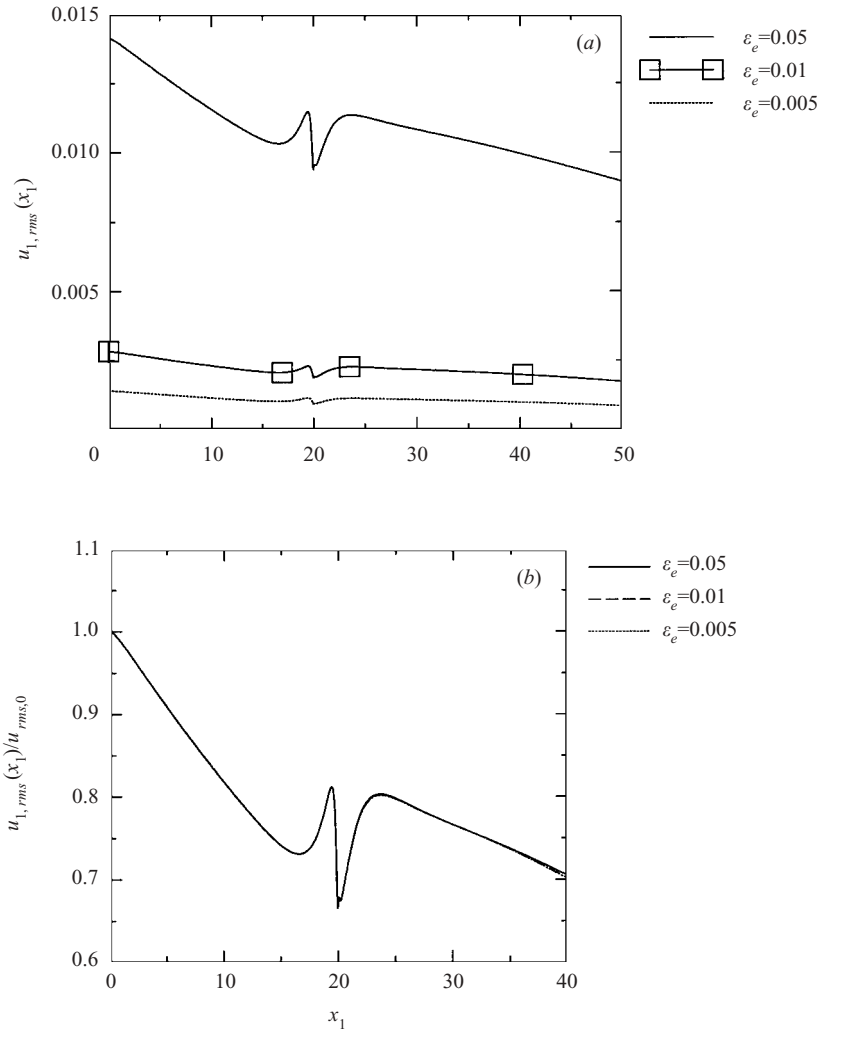


FIGURE 16. Root-mean-square (r.m.s.) variation of u_1 as function of x_1. Results for different perturbation amplitudes ε_e in the inflow plane. (*a*) Absolute r.m.s levels; (*b*) r.m.s. values normalized by the respective values ($u_{rms,0}$) in the inflow plane.

maximum and has about the same magnitude as the mean shear. If the disturbance amplitude is large enough, a superposition of the curves for the fluctuating part and the mean-flow part produces regions where the total shear $\partial u_1/\partial x_2$ is non-negative from the inflow up to the step wall. Such regions are clearly visible in figure 11 around spanwise locations x_2 of about 1.2 and 4.0. On the other hand, for small amplitudes in fluctuating shear, only a weak perturbation of the line of separation will occur.

4.5. *Wavenumber selection*

In all simulations discussed so far, the box size in the spanwise direction was set to about three times the step height, which corresponds to the preferred spanwise spacing of the three-dimensional flow structures. A hint that this preferred length scale may be related to some wavenumber selection process was already gained from the linear stability analysis, which showed the smallest damping rates for wavenumbers around

https://doi.org/10.1017/S0022112003004440 Published online by Cambridge University Press

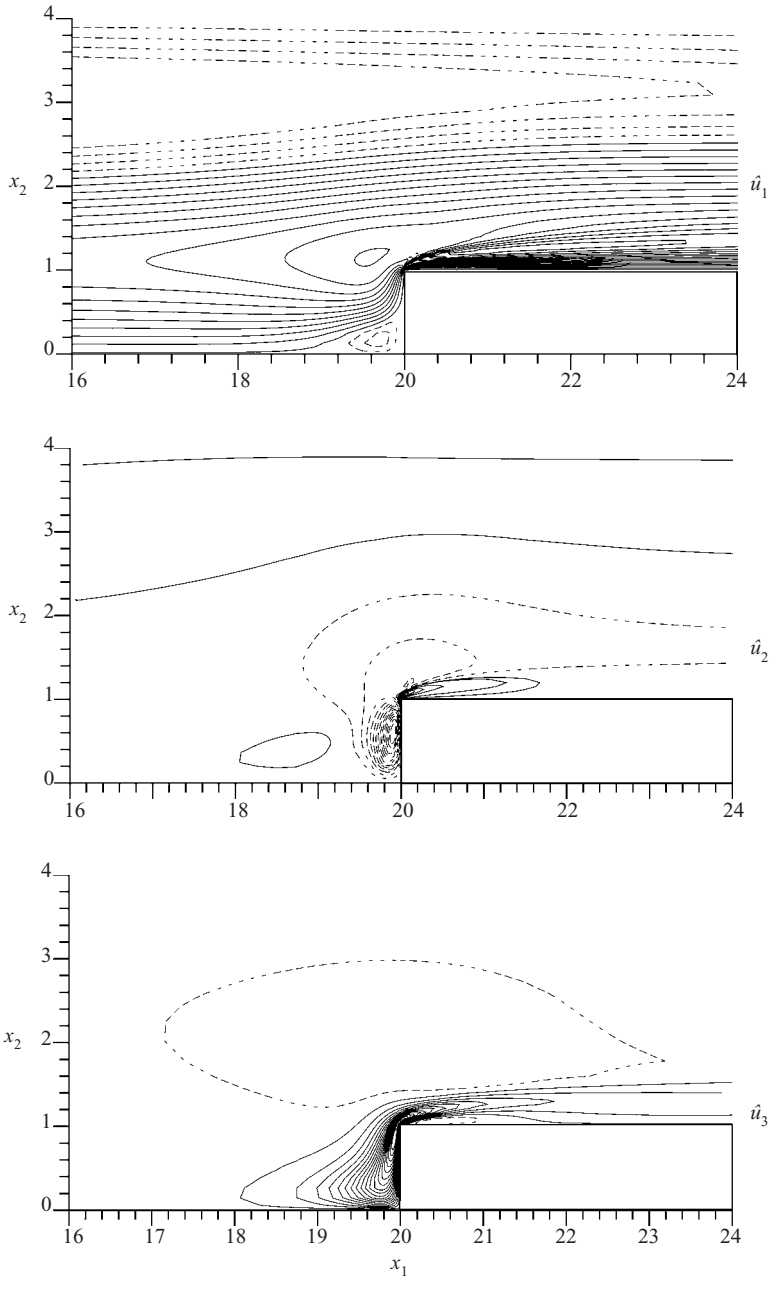


FIGURE 17. Isocontours of the Fourier components $\hat{u}_i$ of the mode $m = 1$. Results for a disturbance amplitude of $\varepsilon_e = 0.05$ in the inflow plane.

$\alpha = 2$. To demonstrate that the same selection mechanism acts on a broadband inflow disturbance spectrum, we conducted simulations with a large number of excited modes in wide boxes of $L_z = 15.71$ and $L_z = 31.41$, respectively. These box widths correspond to fundamental wavenumbers of $\alpha_0 = 0.4$ and 0.2. Here, results will be presented for the first case only, since essentially identical results were obtained in the other case. Thirty complex Fourier modes were employed for the discretization

https://doi.org/10.1017/S0022112003004440 Published online by Cambridge University Press

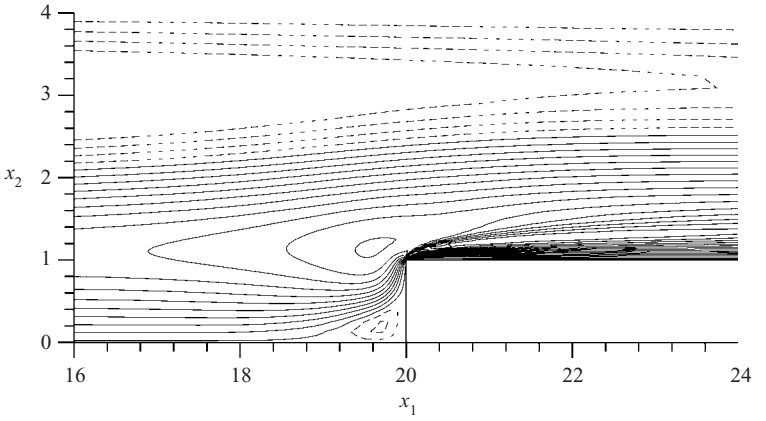


FIGURE 18. Isocontours of the Fourier component $\hat{u}_1$ of the mode $m = 1$. Results for a disturbance amplitude of $\varepsilon_e = 0.005$ in the inflow plane.

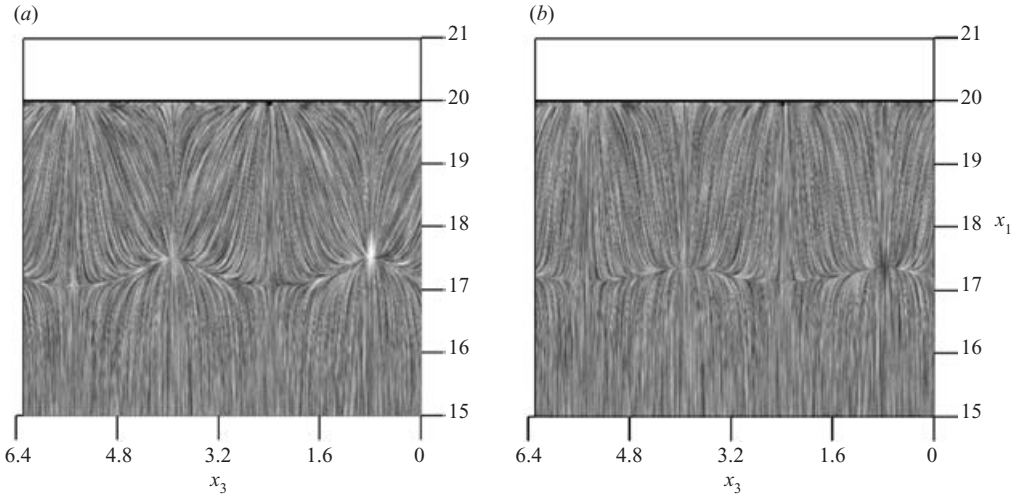


FIGURE 19. Wall-friction lines on the channel floor ahead of the step. Results for different disturbance amplitudes ε_e in the inflow plane (same type of inflow disturbances as for the flow in figure 9). (*a*) $\varepsilon_e = 0.01$, (*b*) $\varepsilon_e = 0.005$.

in the spanwise direction. In the inflow plane perturbations according to (19) were prescribed for all modes, with identical amplitude $\varepsilon_e = 0.03$ but with random phase shifts added to the arguments in the sine function. To quantify the excitation level of each Fourier mode, we computed the following modal energy E_1 of $\hat{u}_1$

$$E_1(x_1, m) = \frac{1}{H} \int_0^H |\hat{u}_1(x_1, x_2, m)|^2 \, \mathrm{d}x_2. \tag{21}$$

In figure 21, the variation of E_1 with x_1 is plotted for all spanwise modes. In the channel section ahead of the step, the curves show that modes with shorter spanwise length scale (that is with higher m) feature higher decay rates. The difference is less pronounced, though, for modes with a length of periodicity much larger than the channel height ($m = 1, 2$), since for such disturbances streamwise and wall-normal velocity gradients play a more important role concerning dissipative losses

https://doi.org/10.1017/S0022112003004440 Published online by Cambridge University Press

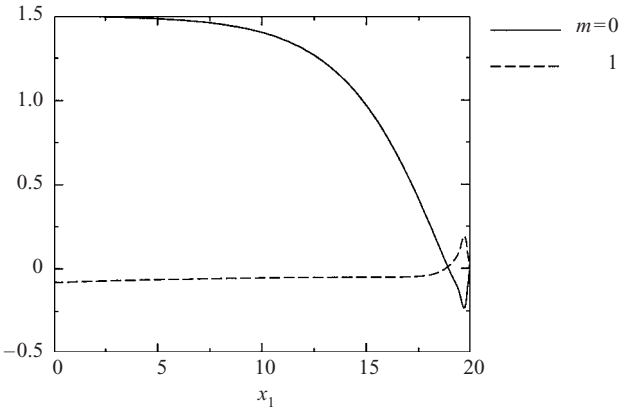


FIGURE 20. Wall-gradient $\partial\hat{u}_1/\partial x_2$ for different Fourier modes. $m=0$ designates the spanwise averaged flow, the solid curve gives the mean shear at the wall. The dashed curve gives the amplitude of the fluctuations in shear $\partial u_1/\partial x_2$ due to the mode $m=1$. Results for a disturbance amplitude of $\varepsilon_e=0.05$ in the inflow plane.

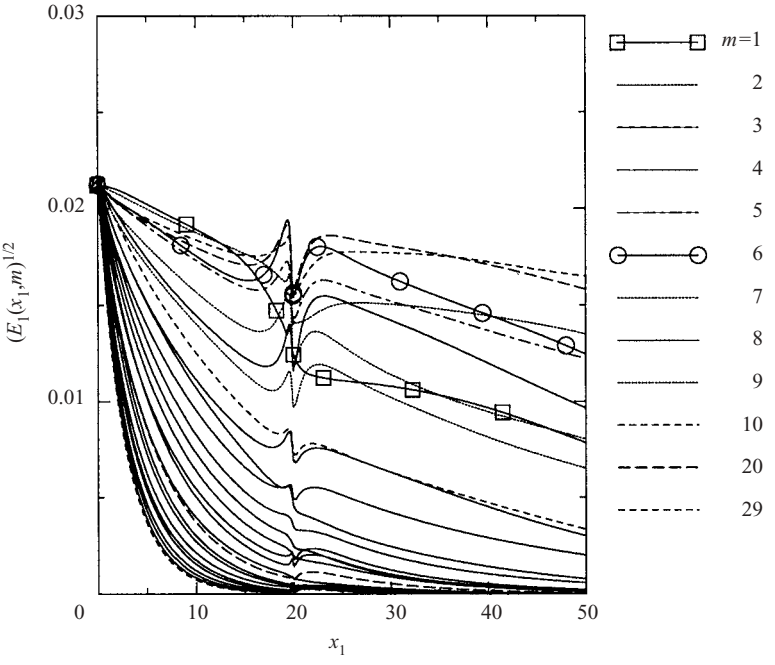


FIGURE 21. Square root of the streamwise mode energy $(E_1(x_1,m))^{1/2}$ for different modes m as a function of x_1. The length of periodicity L_z was set to 15.71 in this simulation ($\alpha_0=0.4$).

than spanwise gradients. The crucial wavenumber selection process at the step is clearly revealed by the pronounced differences between the curves at about $x_1=20$. Modes with wavenumbers around $m=5,6$ experience a much larger increase in amplitude than modes of either shorter or longer wavelength. Given the fundamental wavenumber of $\alpha_z=0.4$, preferential excitation is thus found for disturbances with wavenumbers between 2.0 and 2.4, i.e. with a spanwise scale of about 2.5–3 times the step height. This agrees closely with the linear-stability results presented before, and

https://doi.org/10.1017/S0022112003004440 Published online by Cambridge University Press

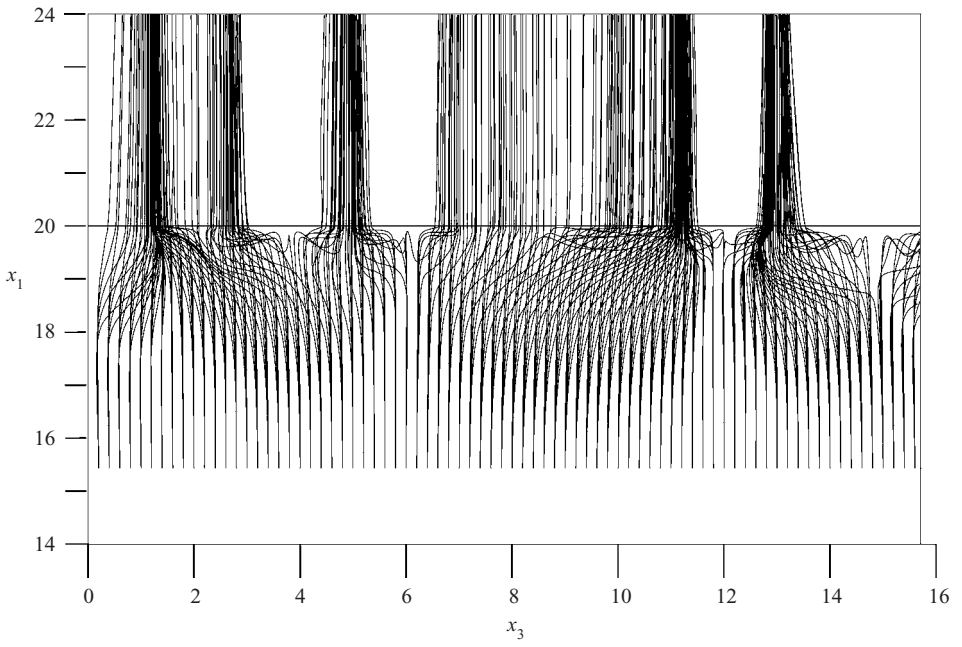


FIGURE 22. Streamlines for wide box simulation with $L_z = 15.71$ ($\alpha_0 = 0.4$).

also with the spacing observed in experiments (see Stüer 1999). This wavenumber selection process is the reason why inflow disturbances in the form of broadband noise still produce a cellular structures with a spacing close to three times the step height at this Reynolds number.

To give an impression of the three-dimensional flow developing in the wide-box simulation, we have evaluated streamlines for the final steady-state velocity field, which are displayed in figure 22. The vortical motion in the separation region ahead of the step is again clearly visible, as well as the characteristic streaks downstream of the step with a dominant spanwise spacing.

5. Summary

We have discussed results from a computational study of laminar forward-facing step flow at a Reynolds number of 330 (based on step height h and bulk velocity of the oncoming flow). The study was conducted to gain better understanding of the pronounced three-dimensionality in the step region that is commonly observed with this flow. The configuration considered is an infinitely extended step in a plane channel of height $H = 4h$. Possible sidewall effects are not taken into account in our study; however, the close agreement between our computational results and the experimental findings suggets that, at least as far as the structure formation at the step is concerned, sidewall effects do not play a critical role.

To clarify whether the three-dimensionality is caused by some absolute instability of the closed separation bubble of the two-dimensional FFS flow, we conducted a linear-stability analysis of the flow in the first part of the paper. The analysis concentrates on the flow in the step region and employs two-dimensional simulation data for the base flow. The response of this base flow to three-dimensional disturbances of small amplitude was then analysed. We presented the relevant stability equations and

https://doi.org/10.1017/S0022112003004440 Published online by Cambridge University Press

briefly outlined the numerical solution method. The stability curve obtained makes clear that in two-dimensional FFS flow small three-dimensional disturbances in the step region and the separation zone decay with time, meaning that – in the present configuration and for the Reynolds number considered – the flow is not absolutely unstable.

The main part of the paper was then devoted to direct simulations of three-dimensional forward-facing step flow, which were initialized with a two-dimensional solution and superimposed perturbations of a different kind and intensity. To be able to capture all relevant flow phenomena accurately, a high-order numerical simulation technique was employed, based on spectral-element and Fourier spectral approaches for the spatial discretization. Consistent with the findings from the stability analysis, the simulations reveal that the two-dimensional–three-dimensional transition in the step region is a not a manifestation of some absolute instability of the separation zone; rather, it is a sensitive reaction of the flow in the step region to incoming disturbances. In consequence, when the disturbances in the oncoming stream are not maintained, the flow unconditionally returns to the two-dimensional state. The response of the flow at the step goes along with a topological change from a two-dimensional closed separation bubble to an open type three-dimensional separation. We demonstrated that disturbance amplitudes of less than 1% of the mean flow intensity (measured at a position of some 10 step heights upstream of the step) already suffice to produce a visibly three-dimensional structure at the step. However, a transition from a pronounced three-dimensional state to almost two-dimensional recirculation is observed if the disturbance level is systematically decreased. Although even for small disturbance amplitudes, the changes in flow topology at the step appear dramatic, the simulations reveal that the three-dimensional structure in the separation region is in fact a linear response of the two-dimensional base flow to small perturbations. The intensity of the three-dimensionality at the step was shown to be proportional to the intensity of the disturbances in the incoming flow. Moreover, we found that, at least for the case considered here, the average properties of forward-facing step flow are well captured by a two-dimensional model. We compared the spanwise-averaged flow field of a three-dimensional simulation with a strictly two-dimensional flow at the same Reynolds number, and found these to be virtually identical.

The simulation results were compared with recent experimental data on the flow topology of forward-facing step flow and close agreement was observed. The characteristic shape of the streamlines in the step region, as well as the formation of streaks downstream of the step edge, are fully reproduced in the computations. In addition, we showed that the pronounced streaks are directly related to pairs of counter-rotating vortices that develop at the step and persist further downstream. Finally, the simulations illustrate how the spanwise spacing of the streaks is an intrinsic scale of the flow which corresponds to a wavenumber selection process acting in the step region. In good agreement with experimental observations, we found the preferred spanwise scale to be about three times the height of the step at the present conditions.

The authors wish to thank Dr A. Gyr, and Dr H. Stüer for helpful discussions. We thank G. Jaquemoud for his assistance with the linear stability analysis. The simulations were performed on the NEC SX-5 system of the Swiss Center for Scientific Computing (CSCS) in Manno.

https://doi.org/10.1017/S0022112003004440 Published online by Cambridge University Press

REFERENCES

Abu-Mulaweh, H. I., Armaly, B. F. & Chen, T. S. 1996*a* Laminar natural convection flow over vertical forward-facing step. *J. Thermophys. Heat Transfer* **10**, 517–523.

Abu-Mulaweh, H. I., Armaly, B. F. & Chen, T. S. 1996*b* Measurements in buoyancy-opposing laminar flow over a vertical forward-facing step. *Int. J. Heat Mass Transfer* **39**, 1805–1813.

Chiba, K., Ishida, R. & Nakamura, K. 1995 Mechanism for entry flow instability through a forward-facing step channel. *J. Non-Newtonian Fluid Mech.* **57**, 271–282.

Chou, J. H. & Chao, S. Y. 2000 Branching of a horseshoe vortex around surface-mounted rectangular cylinders. *Exps Fluids* **28**, 394–402.

Dennis, S. C. R. & Smith, F. T. 1980 Steady flow through a channel with a symmetrical constriction in the form of a step. *Proc. R. Soc. Lond.* A **372**, 393–414.

Dimaczek, G., Kessler, R., Martinuzzi, R. & Tropea, C. 1989 The flow over two-dimensional, surface-mounted obstacles at high Reynolds numbers. In *Proc. 7th Symp. on Turbulent Shear Flows* (ed. F. Durst), pp. 10–11. Stanford.

Drazin, P. G. & Reid, W. H. 1982 *Hydrodynamic Stability*. Cambridge University Press.

Driver, D. M. & Hebbar, S. K. 1989 Three-dimensional sheardriven boundary-layer flow with stream-wise adverse pressure gradient. *AIAA J.* **27**, 1989–1697.

Fischer, P. F. 1997 An overlapping Schwarz method for spectral element solution of the incompressible Navier–Stokes equations. *J. Comput. Phys.* **133**, 84–101.

Gerdes, K. & Schötzau, D. 1999 *hp*-finite element simulations for Stokes flow – stable and stabilized. *Finite Elem. Anal. Des.* **33**, 143–165.

Graf, F., Meiburg, E. & Härtel, C. 2002 Density-driven instabilities of miscible fluids in a Hele-Shaw cell: linear stability analysis of the three-dimensional Stokes equations. *J. Fluid Mech.* **451**, 262–281.

Härtel, C., Carlsson, F. & Thunblom, M. 2000 Analysis and direct numerical simulation of the flow at a gravity current head. Part 2. The lobe-and-cleft instability. *J. Fluid Mech.* **418**, 213–229.

Huerre, P. & Monkewitz, P. A. 1990 Local and global instabilities in spatially developing flows. *Annu. Rev. Fluid Mech.* **22**, 473–537.

Kaiktsis, L., Karniadakis, G. E. & Orszag, S. A. 1991 Onset of three-dimensionality, equilibria, and early transition in flow over a backward-facing step. *J. Fluid Mech.* **231**, 501–528.

Karniadakis, G. M., Israeli, M. & Orszag, S. A. 1991 High-order splitting methods for the incompressible Navier–Stokes equations. *J. Comput. Phys.* **97**, 414–443.

Maday, Y. & Patera, A. T. 1989 Spectral element methods for the incompressible Navier–Stokes equations. In *State-ofthe-Art-Surveys in Computational Mechanics* (ed. A. K. Noor), pp. 71–143. ASME, New York.

Mei, R. W. & Plotkin, A. 1986 Navier–Stokes solutions for laminar incompressible flows in forward-facing step geometries. *AIAA J.* **24**, 1106–1111.

Pollard, A., Wakarani, N. & Shaw, J. 1996 Genesis and morphology of erosional shapes associated with turbulent flow over a forward-facing step. In *Coherent Flow Structures in Open Channels* (ed. P. J. Ashworth), pp. 249–265. John Wiley.

Robinson, S. K. 1991 Coherent motions in the turbulent boundary layer. *Annu. Rev. Fluid. Mech.* **23**, 601–639.

Shakouchi, T. & Kajino, I. 1993 Flow and forced-convection heat transfer over forward-facing double steps (effects of step ratio). *Heat Transfer–Japan. Res.* **22**, 716–730.

Smith, F. T. 2000 On physical mechanisms in two- and three-dimensional separations. *Phil. Trans. R. Soc. Lond.* A **358**, 3091–3111.

Smith, F. T. & Walton, A. G. 1998 Flow past a two- or three-dimensional steep-edged roughness. *Proc. R. Soc. Lond.* A **454**, 31–69.

Sorensen, D. C. 1992 Implicit application of polynomial filters in a k-step Arnoldi method. *SIAM J. Matrix Anal. Applic.* **13**, 357–385.

Stewart, P. A. & Smith, F. T. 1987 Three-dimensional instabilities in steady and unsteady non-parallel boundary layers, including effects of Tollmien–Schlichting disturbances and cross flow. *Proc. R. Soc. Lond.* A **409**, 229–248.

Stüer, H. 1999 *Investigation of Separation on a Forward Facing Step*. PhD thesis 13132, ETH Zürich.

https://doi.org/10.1017/S0022112003004440 Published online by Cambridge University Press

Stüer, H., Gyr, A. & Kinzelbach, W. 1999 Laminar separation on a forward facing step. *Eur. J. Mech.* B/*Fluids* **18**, 675–692.

Theofilis, V., Hein, S. & Dallmann, U. 2000 On the origins of unsteadiness and three-dimensionality in a laminar separation bubble. *Phil. Trans. R. Soc. Math. Phys. Engng Sci.* **1777**, 3229–3246.

Watanabe, K. & Kamiya, N. 1996 The axial flow around a circular cylinder with a forward facing step. *Trans. Japan Soc. Aero. Space Sci.* **39**, 222–230.

Werner, H. & Wengle, H. 1989 Large-eddy simulation of turbulent flow over a square rib in a channel. In *Advances in Turbulence 2* (ed. H. H. Fernholz), pp. 418–423. Springer.

Wilhelm, D. 2000 *Numerical investigation of three-dimensional separation in a forward-facing step flow using a spectral element method*. PhD thesis 13774, ETH Zürich. Also published as *Fortschritt Bericht 7-404*, VDI, Düsseldorf, Germany.

Wilhelm, D., Härtel, C. & Eckelmann, H. 1998 On the relation between fronts and high-shear layers in wall turbulence. *Flow Turbul. Combust.* **60**, 87–103.

Wilhelm, D. & Kleiser, L. 2000 Stable and unstable formulation of the convection operator in spectral element simulations. *Appl. Numer. Maths* **33**, 275–280.

Wilhelm, D. & Kleiser, L. 2001 Stability analysis for different formulations of the nonlinear term in P_N–P_{N-2} spectral element discretizations of the Navier–Stokes equations. *J. Comput. Phys.* **174**, 306–326.

Wilhelm, D. & Kleiser, L. 2002 Application of spectral element method to 2D forward facing step flow. *J. Sci. Comput.* **17**, 619–627.

https://doi.org/10.1017/S0022112003004440 Published online by Cambridge University Press